Drug Delivery

International Edition: DOI: 10.1002/anie.201510409
German Edition: DOI: 10.1002/ange.201510409

Tailored Synthesis of Octopus-type Janus Nanoparticles for Synergistic Actively-Targeted and Chemo-Photothermal Therapy

Lingyu Zhang[+], Yinyin Chen[+], Zilu Li, Lu Li, Philippe Saint-Cricq, Chunxia Li,* Jun Lin, Chungang Wang,* Zhongmin Su, and Jeffrey I. Zink*

Abstract: *A facile, reproducible, and scalable method was explored to construct uniform Au@poly(acrylic acid) (PAA) Janus nanoparticles (JNPs). The as-prepared JNPs were used as templates to preferentially grow a mesoporous silica ($mSiO_2$) shell and Au branches separately modified with methoxy-poly(ethylene glycol)-thiol (PEG) to improve their stability, and lactobionic acid (LA) for tumor-specific targeting. The obtained octopus-type PEG-Au-PAA/$mSiO_2$-LA Janus NPs (PEG-OJNP-LA) possess pH and NIR dual-responsive release properties. Moreover, DOX-loaded PEG-OJNP-LA, upon 808 nm NIR light irradiation, exhibit obviously higher toxicity at the cellular and animal levels compared with chemotherapy or photothermal therapy alone, indicating the PEG-OJNP-LA could be utilized as a multifunctional nanoplatform for in vitro and in vivo actively-targeted and chemo-photothermal cancer therapy.*

Janus nanoparticles (JNPs) have attracted considerable attention owing to their anisotropic surface properties and various functionalities that allow them to house several components for cancer detection and targeting.[1] Specifically, polymer/metal hybrid JNPs spontaneously integrated the significant distinguished and complementary properties of inorganic and organic domains for diverse applications.[2] Amongst these, polymer/Au JNPs are of great interest in the field of their potential use in clinical diagnosis, biotechnology, and drug delivery.[3] However, the synthetic techniques for polymer/Au JNPs were either in complex and multistep procedures which were time-consuming, uneconomical, and unsuitable for large-scale production, in need of various types of polymers, or precisely controlled thermodynamic process in which the size and structure of the resulting JNPs could not be exactly controlled.[3a,4] Therefore, the major challenge in the field is not only to discover facile, mild, and reproducible synthetic strategies directly from solution to fabricate polymer/Au JNPs on large scale, but also to further grow complex asymmetric nanostructures with unique morphology and tailored optical properties in a controlled manner using polymer/Au JNPs as seeds.

Owing to the combination of two distinct sides with different materials in one single unit and the asymmetry in surface chemistry, JNPs have more room to perform different functions for cancer therapy compared with the traditional core–shell NPs.[1d,5] During the past decades, in spite of the remarkable progress in the development of multifunctional core–shell NPs as therapeutic agents for cancer treatment,[6] the integration of pH-near infrared (NIR) light dual-responsive properties and specific targeting in a single polymer/Au-based multifunctional JNP for in vitro and in vivo snyergistic chemo-photothermal cancer therapy have not been explored yet.

Herein, we present a reproducible, facile, and scalable strategy to generate uniform Au@poly(acrylic acid) (PAA) JNPs under mild conditions, which were further employed as templates to preferentially coat a mesoporous silica ($mSiO_2$) shell on the side of the PAA and selectively grow Au branches on the other Au side, respectively. Selectively modified with methoxy-poly(ethylene glycol)-thiol (PEG) and lactobionic acid (LA) on the distinguished domains could improve their stability, biocompatibility, blood circulation time, and specifically target hepatocytes or hepatoma cells bearing asialoglycoprotein receptors.[7] The obtained multifunctional octopus-type PEG-Au-PAA/$mSiO_2$-LA Janus NPs (PEG-OJNP-LA) were designed to integrate NIR light and pH dual-stimuli responsive properties, drug loading capacity, photothermal effect, and specific tumor-targeting into one single PEG-OJNP-LA, which can act as an efficient multifunctional nanoplatform for actively-targeted chemo-photothermal synergistic cancer therapy in vitro and in vivo (Scheme 1).

The citrate-Au NPs with mean diameter $\approx$50 nm were prepared by a reported method (Figure 1 A).[8] The obtained Au NPs were mixed with PAA and aqueous ammonium hydroxide in water, and then isopropyl alcohol (IPA) was added to generate monodispersed Au-PAA JNPs consisting of approximately 50 nm Au and 70 nm PAA with spherical shape. Additionally, the Au-PAA JNPs with different thickness of PAA shells (20 nm, 37 nm and 70 nm) could be easily obtained by adjusting the amounts of PAA in the initial mixture (Supporting Information, Figure S1). Importantly, the synthesis was found to be very reproducible and scalable, and all of the Au NPs had partial PAA shells with highly

[*] Dr. L. Zhang,[+] Dr. L. Li, Prof. C. Wang, Prof. Z. Su
Department of Chemistry, Northeast Normal University
5268 Renmin Street, Changchun, Jilin, 130024 (P. R. China)
E-mail: lil106@nenu.edu.cn
wangcg925@nenu.edu.cn
Y. Chen,[+] Prof. C. Li, Prof. J. Lin
State Key Laboratory of Rare Earth Resource Utilization
Changchun Institute of Applied Chemistry
Chinese Academy of Sciences
Changchun 130021 (P. R. China)
E-mail: cxli@ciac.ac.cn
Z. Li, Dr. P. Saint-Cricq, Prof. J. I. Zink
Department of Chemistry and Biochemistry
University of California, Los Angeles
609 Charles E. Yong Dr. E, Los Angeles, CA 90095 (USA)
[+] These authors contributed equally to this work.

Supporting information for this article is available on the WWW under http://dx.doi.org/10.1002/anie.201510409.

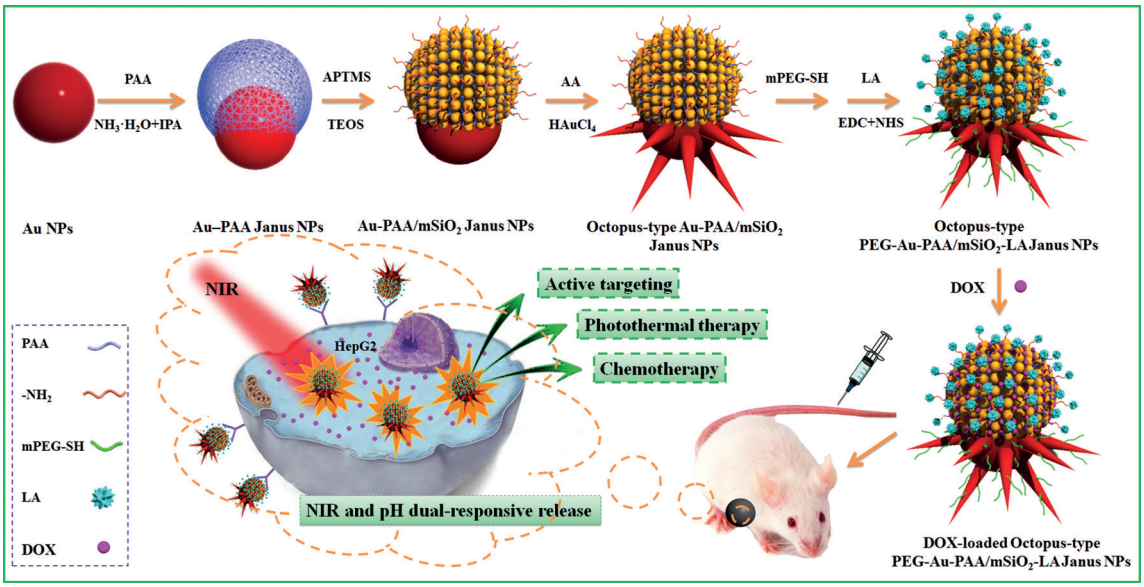

Scheme 1. Fabrication of octopus-type PEG-Au-PAA/mSiO$_2$-LA Janus NPs (PEG-OJNP-LA) with pH and NIR light dual-stimuli responsive properties for actively-targeted and chemo-photothermal cancer therapy in vitro and in vivo.

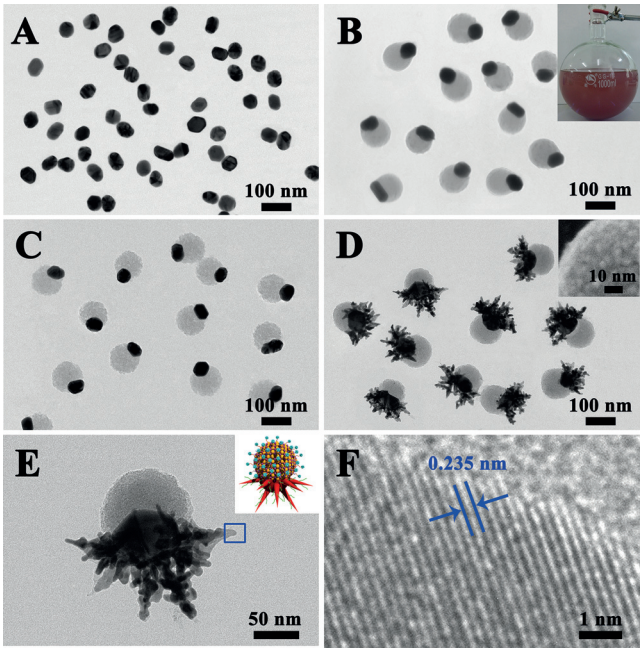

Figure 1. TEM images of A) Au NPs and B) Au-PAA JNPs, inset presents the product of the scaled-up synthesis (750 mL). C) Au-PAA/mSiO$_2$ JNPs and D) PEG-OJNP-LA, inset is the magnified SEM image of the mSiO$_2$ surface. E) HRTEM image of a single PEG-OJNP-LA and F) magnified HRTEM image of square-marked region in E.

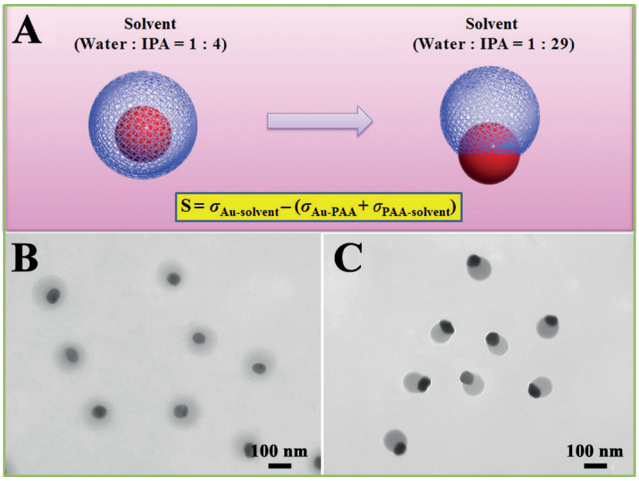

Figure 2. A) The solvent-induced structure transformation and corresponding TEM images: B) Au-PAA core–shell NPs, and C) Au-PAA JNPs.

uniformed Janus structure (> 99 %), and large scale production could be easily obtained (Figure 1 B). Interestingly, when increasing the ratio of water to IPA from 1:4 to 1:29, a structure transition was observed from Au-PAA core–shell NPs to Au-PAA JNPs (Figure 2 A). The complete engulfing of Au NPs by PAA transformed to partial engulfing is correlated with the change of the interfacial energy $\sigma_{\text{Au-PAA}}$, $\sigma_{\text{PAA-solvent}}$, and $\sigma_{\text{Au-solvent}}$.[9] When the ratio of water to IPA is 1:4, the Au-PAA core–shell NPs are prepared, $S = \sigma_{\text{Au-solvent}} - (\sigma_{\text{Au-PAA}} + \sigma_{\text{PAA-solvent}}) > 0$, where S is the spreading coefficient. When more IPA was added to the suspension (water to IPA = 1:29), the $\sigma_{\text{Au-solvent}}$ and $\sigma_{\text{PAA-solvent}}$ decrease proportionally. However, the decrease of $\sigma_{\text{Au-solvent}}$ is more than that of $\sigma_{\text{PAA-solvent}}$ owing to $S < 0$, resulting in the partial engulfing of Au NPs, which is confirmed by transmission electron microscopic (TEM) images (Figure 2 B and C).

As PAA can absorb and reserve water molecules inside its net structure, tetraethyl orthosilicate (TEOS) is spatio-selectively hydrolyzed in the PAA network to generate the semi-PAA/SiO$_2$ nanoclusters (Figure 1 C), which consist of a large amount of small SiO$_2$ NPs with aggregate mesoporous pores leaving the Au surface untouched, confirmed by a magnified scanning electron microscope (SEM) image (Figure 1 D). Meanwhile, 3-aminopropyltrimethoxysilane (APTMS) was added to modify the mSiO$_2$ domain with amino group for further functionalization. Then, the PAA/mSiO$_2$ semi-shell serves as a mask to guide the subsequent

seeded growth of Au branches on the exposed domain of Au by a surfactant free method without self-nucleation in an aqueous solution, thus forming the octopus-type Au-PAA/$mSiO_2$ Janus NPs (OJNPs) (Figure 1E), where L-ascorbic acid was used as a reducing agent in the presence of $HAuCl_4$, $AgNO_3$, and HCl. Note that, owing to the absence of surfactant during the growing process of Au spikes, their surface is readily available for further modification with PEG. Compared to non-modified OJNPs, no precipitation of PEG modified OJNPs in water, PBS, or culture medium occurred within 24 h (Figure S2), indicating their good stability. Then, LA was linked to the surface of the PAA/$mSiO_2$ by using EDC/NHS as coupling agents. The successful preparation and modification were further indicated by the Fourier transform infrared spectra (Figure S3). High-resolution TEM (HRTEM) images of a PEG-OJNP-LA presented the well-defined lattice fringes with a d-spacing of 0.235 nm, which corresponds to the (111) planes of Au, confirming the presence of Au (Figure 1F). The amount of Au and Si in weight percent, measured by an inductively coupled plasma mass spectrometry, were found to be 89.7 and 2.6, respectively. The N_2 adsorption/desorption isotherms of PEG-OJNP-LA exhibited type-IV curves (Figure S4). The surface area and pore volume were estimated to be 345.3 $m^2 g^{-1}$ and 0.213 $cm^3 g^{-1}$ by BET, and the average pore diameter $\approx$2 nm was measured by BJH method, indicating the porous structure and possibility for drug loading.

To prove that the PEG-OJNP-LA could be used for photothermal therapy (PTT), the localized surface plasmon resonance was measured at 794 nm in NIR region (Figure S5), and the η value was calculated to be 49.5% according to the previous report (Figure S6).[10] With the 808 nm NIR light irradiation for 300 s (2 W cm^{-2}), the temperature of 0.2 mg mL^{-1} PEG-OJNP-LA solution greatly increased to 60 °C, and the water only changed by 2 °C, implying that the PEG-OJNP-LA are responsible for the temperature increase (Figure S7). After heating, the TEM image in Figure S8 proved that the PEG-OJNP-LA stay unchanged. Moreover, the in vitro experiments showed that no cell was killed in the PEG-OJNP-LA or NIR light only groups in 24 h. In contrast, most of the cells were destroyed inside the region of laser spot when treated with PEG-OJNP-LA (Figure S9).

After loading doxorubicin hydrochloride (DOX) into the PEG-OJNP-LA with high loading efficiency $\approx$90% (loading capacity = 0.36 mg DOX/mg PEG-OJNP-LA; Figure S10), they were dispersed in PBS buffer (pH 5.1) at 37 °C upon NIR light irradiation for 5 min at different time intervals. An enhanced rate of release of DOX (95%) was observed within 60 min, which was about 2.6-fold higher than the pH 5.1 without NIR light group (41%), and 12.3-fold higher than the pH 7.4 group (9%). Such significantly enhanced DOX release was caused by both the protonation of the pH-dependent polymer PAA and the remote heating produced by the PEG-OJNP-LA by photothermal conversion, thus realizing pH and NIR dual-stimuli responsive release (Figure 3A). The MTT assay on HepG2 cells further confirmed that combination of DOX/PEG-OJNP-LA with NIR laser irradiation induced the greatest cell death (94%) compared with other groups within 24 h, but the pure NPs did not have significant toxicity

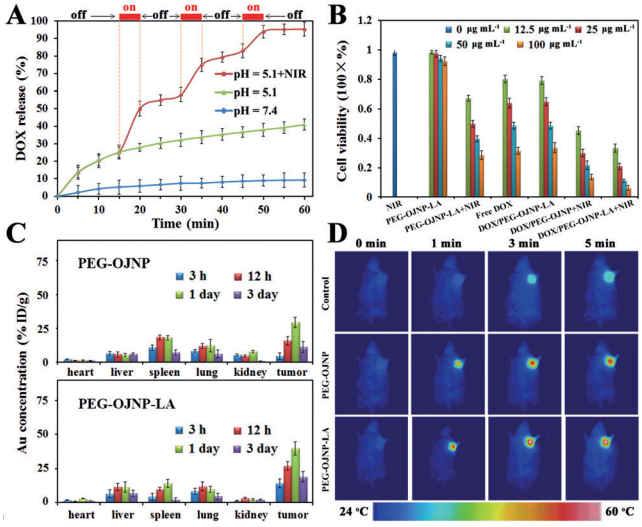

Figure 3. A) Release profiles of DOX/PEG-OJNP-LA in different situations. B) MTT cell viability assay of HepG2 cancer cells with different treatments. C) Biodistribution in tissues of mice after injection for different times. D) Infrared thermal images of H-22-tumor-bearing Kunming mice with different treatments.

(Figure 3B), implying the combination of controlled drug release, active targeting, chemotherapy, and PTT showed remarkable synergistic therapeutic effect with fewer side effect.

To exam the impact of active targeting, the cellular uptake showed that the PEG-OJNP-LA in HepG2 cells presented the highest fluorescence compared to the PEG-OJNP-LA in LA receptor negative Hela cells and non-targeted octopus-type PEG-Au-PAA/$mSiO_2$ Janus NPs (PEG-OJNP) in HepG2 cells after 3 h incubation (Figure S11). Additionally, the biodistribution showed that the PEG-OJNP were mainly in the spleen and liver at 3 h post injection, but the PEG-OJNP-LA showed more-significant accumulation at the tumor site (Figure 3C). With NIR light irradiation for 5 min, the infrared thermal camera images showed that the local surface temperature of tumors treated with PEG-OJNP increased steadily with the increase of irradiation time, however the temperature of tumors treated with PEG-OJNP-LA increased (> 60 °C) significantly enough for heat-induced tumor inhibition (Figure 3D). In comparison, the tumor treated with PBS only reached 34 °C. These results confirmed the active targeting capability of PEG-OJNP-LA in vitro and in vivo.

To evaluate the in vivo therapeutic effect, sixteen H-22-tumor-bearing Kunming mice were randomly separated into 5 groups for different treatment. There was no statistically significant difference in the weight changes among these groups within 11 days (Figure 4A). However, the tumor volume of the control group exhibited a rapid increase compared with other groups (Figure 4B). After 11 days, all of the mice were sacrificed and the tumors were collected (Figure 4C) and weighed to evaluate the tumor inhibition rates. The mice injected with DOX/PEG-OJNP-LA upon NIR light showed highest tumor suppression of about 98%, compared to DOX/PEG-OJNP with NIR light (91%), DOX/PEG-OJNP-LA (81%), and free DOX treated group (46%) (Figure S12), implying the effective synergistic effect in vivo.

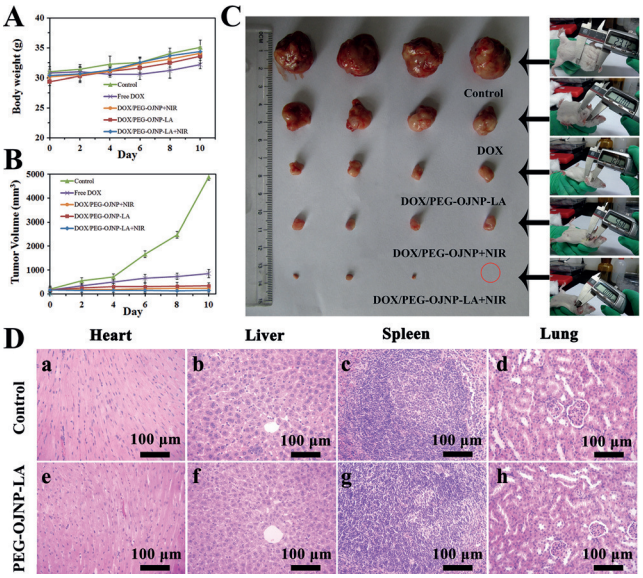

Figure 4. Change in A) body weight and B) relative tumor volume from the H-22-tumor-bearing Kunming mice with different treatment. C) Representative photograph of excised tumors from euthanatized mice at 11 days post treatment. D) Hematoxylin- and eosin-stained images of major organ tissues from mice after 11 days post injection with PBS (control) and PEG-OJNP-LA.

Furthermore, the histological assessment confirmed that there was no damage or inflammation in the major organs after injection of PEG-OJNP-LA with (Figure S13) or without (Figure 4D) DOX, suggesting their excellent biocompatibility and fewer side effects for cancer therapy.

In summary, we explored a facile, reproducible, and scalable method to construct uniform nano-sized Au-PAA Janus structure NPs, which were further employed to preferentially grow $mSiO_2$ and Au branches forming unique OJNPs. Modification with PEG and LA significantly improved their biocompatibility and tumor targeting. The obtained PEG-OJNP-LA not only possess high drug loading, but also pH and NIR dual-responsive release properties. Moreover, DOX-loaded PEG-OJNP-LA upon 808 nm NIR light irradiation exhibit higher toxicity at cellular and animal levels compared with chemotherapy or PTT alone, indicating the effectiveness of the combined chemo-photothermal cancer therapy. Furthermore, this synthetic strategy could be extended to synthesize other kinds of JNPs. Taken together, such multifunctional PEG-OJNP-LA provide an intriguing nanoplatform for synergistic actively-targeted and chemo-photothermal cancer therapy, which will undoubtedly aid in the development of a new generation of cancer treatment materials in the future.

Acknowledgements

We would like to thank the National Natural Science Foundation of China (21573040, 21173038, 21301027, 51422209, and 51332008), National Hi-Tech Research and Development Program of China ("863" Project, 2013AA032204), Jilin Provincial Key Laboratory of Advanced Energy Materials (Northeast Normal University), Natural Science Foundation and Science and Technology Development Planning of Jilin Province (20130522136JH, 20140520088JH), Program for New Century Excellent Talents in University (NCET-13-0720), China Postdoctoral Science Foundation funded project (2014M551155, 2015T80283).

Keywords: active targeting · chemo-photothermal therapy · dual-stimuli responsive release · octopus-type Janus nanoparticles

How to cite: *Angew. Chem. Int. Ed.* **2016**, *55*, 2118–2121
Angew. Chem. **2016**, *128*, 2158–2161

[1] a) M. Feyen, C. Weidenthaler, F. Schüth, A. H. Lu, *J. Am. Chem. Soc.* **2010**, *132*, 6791–6799; b) J. Ge, Y. Hu, T. Zhang, Y. Yin, *J. Am. Chem. Soc.* **2007**, *129*, 8974–8975; c) J. Hu, S. Zhou, Y. Sun, X. Fang, L. Wu, *Chem. Soc. Rev.* **2012**, *41*, 4356–4378; d) A. Walther, A. H. E. Müller, *Chem. Rev.* **2013**, *113*, 5194–5261.

[2] a) S. Xing, Y. Feng, Y. Y. Tay, T. Chen, J. Xu, M. Pan, J. He, H. H. Hng, Q. Yan, H. Chen, *J. Am. Chem. Soc.* **2010**, *132*, 9537–9539; b) B. J. Park, T. Brugarolas, D. Lee, *Soft Matter* **2011**, *7*, 6413–6417.

[3] a) T. Chen, M. Yang, X. Wang, L. H. Tan, H. Chen, *J. Am. Chem. Soc.* **2008**, *130*, 11858–11859; b) L. Cheng, C. Wang, L. Feng, K. Yang, Z. Liu, *Chem. Rev.* **2014**, *114*, 10869–10939; c) T. Ding, S. K. Smoukov, J. J. Baumberg, *J. Mater. Chem. C* **2014**, *2*, 8745–8749; d) Y. Wang, T. Ding, J. J. Baumberg, S. K. Smoukov, *Nanoscale* **2015**, *7*, 10344–10349.

[4] a) A. Ohnuma, E. C. Cho, P. H. C. Camargo, L. Au, B. Ohtani, Y. Xia, *J. Am. Chem. Soc.* **2009**, *131*, 1352–1353; b) J. He, Y. Liu, T. C. Hood, P. Zhang, J. Gong, Z. Nie, *Nanoscale* **2013**, *5*, 5151–5166.

[5] a) X. Li, L. Zhou, Y. Wei, A. M. El-Toni, F. Zhang, D. Zhao, *J. Am. Chem. Soc.* **2014**, *136*, 15086–15092; b) L. T. C. Tran, S. Lesieur, V. Faivre, *Expert Opin. Drug Delivery* **2014**, *11*, 1061–1074.

[6] a) M. Chen, S. Tang, Z. Guo, X. Wang, S. Mo, X. Huang, G. Liu, N. Zheng, *Adv. Mater.* **2014**, *26*, 8210–8216; b) Z. Zhang, L. Wang, J. Wang, X. Jiang, X. Li, Z. Hu, Y. Ji, X. Wu, C. Chen, *Adv. Mater.* **2012**, *24*, 1418–1423; c) Q. Xiao, X. Zheng, W. Bu, W. Ge, S. Zhang, F. Chen, H. Xing, Q. Ren, W. Fan, K. Zhao, Y. Hua, J. Shi, *J. Am. Chem. Soc.* **2013**, *135*, 13041–13048; d) M. Chen, S. Yang, X. He, K. Wang, P. Qiu, D. He, *J. Mater. Chem. B* **2014**, *2*, 6064–6071; e) M. Chen, P. Qiu, X. He, K. Wang, S. Chen, S. Yang, X. Ye, *J. Mater. Chem. B* **2014**, *2*, 3204–3213; f) G. Yang, R. Lv, F. He, F. Qu, S. Gai, S. Du, Z. Wei, P. Yang, *Nanoscale* **2015**, *7*, 13747–13758; g) M. Liong, J. Lu, M. Kovochich, T. Xia, S. G. Ruehm, A. E. Nel, F. Tamanoi, J. I. Zink, *ACS Nano* **2008**, *2*, 889–896.

[7] H. Liu, H. Wang, Y. Xu, R. Guo, S. Wen, Y. Huang, W. Liu, M. Shen, J. Zhao, G. Zhang, X. Shi, *ACS Appl. Mater. Interfaces* **2014**, *6*, 6944–6953.

[8] N. G. Bastús, J. Comenge, V. Puntes, *Langmuir* **2011**, *27*, 11098–11105.

[9] a) S. Torza, S. G. Mason, *J. Colloid Interface Sci.* **1970**, *33*, 67–83; b) L. Li, L. Zhang, S. Xing, T. Wang, S. Luo, X. Zhang, C. Liu, Z. Su, C. Wang, *Small* **2013**, *9*, 825–830.

[10] P. Huang, P. Rong, J. Lin, W. Li, X. Yan, M. G. Zhang, L. Nie, G. Niu, J. Lu, W. Wang, X. Chen, *J. Am. Chem. Soc.* **2014**, *136*, 8307–8313.

Received: November 9, 2015
Revised: December 7, 2015
Published online: January 6, 2016

